Crossover in periodic length dependence of thermal conductivity in 5d element substituted Fe$_2$VAl-based superlattices

Seongho Choi [1,*] Satoshi Hiroi [2] Manabu Inukai,[1] Shunsuke Nishino [1] Robert Sobota,[1] Dogyun Byeon [1]
Masashi Mikami [3] Emi Minamitani,[4] Masaharu Matsunami,[1] and Tsunehiro Takeuchi[1,5,*]

[1]*Toyota Technological Institute, 2-12-1, Hisakata, Tempaku-ku, Nagoya, Aichi 468-8511, Japan*
[2]*National Institute for Materials Science, 1-1-1, Koto, Sayo, Sayo District, Hyogo 679-5148, Japan*
[3]*National Institute of Advanced Industrial Science and Technology, 2266-98, Anagahora, Shimoshidami,*
Moriyama-ku, Nagoya, Aichi 463-8560, Japan
[4]*Institute for Molecular Science, 38, Nishigo-Naka, Myodaiji, Okazaki, Aichi 444-8585, Japan*
[5]*CREST, Japan Science and Technology Agency, Tokyo, 102-0076, Japan*
and Institute of Innovation for Future Society, Nagoya University, Nagoya, Aichi 464-8603, Japan

We investigated the 5d element substitution effect on the thermal conductivity in Fe$_2$VAl-based superlattice thin films epitaxially grown on a MgO (100) substrate. We found unique crossover behavior in the period dependences of thermal conductivity for Ta-free Fe$_2$VAl and Fe$_2$(V, Ta)Al-based superlattices. The Fe$_2$(V, Ta)Al-based superlattices with periods more than 40 nm appeared to have much lower thermal conductivity than Ta-free Fe$_2$VAl-based superlattices due to the substitution of V by Ta. Unexpectedly, at a shorter periodic length, less than 20 nm, Fe$_2$(V, Ta)Al-based superlattices appeared to have higher thermal conductivity than Ta-free Fe$_2$VAl-based superlattices despite such a heavy element substitution by Ta. This surprising experimental fact was well accounted for with theoretical calculations, which predicted the dominant contribution of phonons having a shorter mean free path in the Ta substituted samples.

I. INTRODUCTION

Fe$_2$VAl-based thermoelectric (TE) materials of $L2_1$-type Heusler phase have been intensively investigated as one of the most promising TE materials. It is widely known that the efficiency of energy conversion in TE generators is an increasing function of the dimensionless figure of merit, $zT = S^2\sigma T/(\kappa_e + \kappa_l)$, of constituent TE materials, where S, σ, κ_e, and κ_l represent the Seebeck coefficient, electrical conductivity, electron thermal conductivity, and lattice thermal conductivity, respectively. All the constituent elements of Fe$_2$VAl are nontoxic and abundant, and this characteristic is an important advantage for mass production. Its power factor ($PF = S^2\sigma$) reaches 6.8 mW m^{-1} K^{-2} at the appropriate carrier concentration, and notably this number is larger than that of Bi$_2$Te$_3$-based TE materials [1,2]. However, the large lattice thermal conductivity of Fe$_2$VAl-based TE materials exceeding 10 W m^{-1} K^{-1} has prevented us from obtaining a good dimensionless figure of merit larger than 0.5. Efforts to effectively reduce the large lattice thermal conductivity, including heavy element substitutions, reduction in grain size, high-pressure torsion, and thin-film processes, have not achieved a significant reduction below 3 W m^{-1} K^{-1} [3–9].

It would be worthwhile mentioning that Hinterleitner *et al.* [10] surprisingly reported that they achieved $zT_{\text{appr}} \sim 5$ in the temperature range of 350–400 K by obtaining not only a huge power factor of more than 40 mW m^{-1} K^{-2} but also low

thermal conductivity of 3.02 W K^{-1} m^{-1} for a Fe$_2$V$_{0.8}$W$_{0.2}$Al single-layer thin film grown on a Si substrate. This report has motivated many researchers to further reduce the lattice thermal conductivity of Fe$_2$VAl.

Takeuchi *et al.* experimentally demonstrated that the lattice thermal conductivity of Fe$_2$VAl is effectively reduced by means of heavy element partial substitutions without seriously altering their electrical properties, provided that the substituting element is carefully selected so as not to produce impurity states near the chemical potential [3,4]. It was clearly shown that 5d heavy transition element substitutions in Fe$_2$VAl led to the lattice thermal conductivity of $\sim$6 W m^{-1} K^{-1} and the value of zT increased up to 0.25 [3,4]. Renard *et al.* also reported that the lattice thermal conductivity of $\sim$5 W m^{-1} K^{-1} can be obtained from Ta substituted Fe$_2$VAl with an off-stoichiometric effect [6].

The thin-film approaches opened another possibility to reduce lattice thermal conductivity. Both Yamada *et al.* [11] and Kudo *et al.* [12] reported the relatively reduced thermal conductivity to be $\sim$7.5 W m^{-1} K^{-1} for Fe$_2$VAl thin films epitaxially grown by means of molecular beam epitaxy techniques. Fukatani *et al.* [7] also reported $\sim$3.8 W m^{-1} K^{-1} for a Fe$_2$VAl thin film with an off-stoichiometric chemical composition fabricated using a direct current magnetron sputtering method.

The use of a well-ordered superlattice is considered as another way for effectively reducing lattice thermal conductivity. In some superlattice systems, notably, a minimum in the thermal conductivity at a periodic length of a few nanometers corresponding to a coherent-incoherent phonon crossover

was reported in the literature [13–21]. The origin of such a nontrivial effect for the thermal transport has not reached the general consensus so far, but it was reported that superlattices with the nanoscaled period are effective for the reduction of thermal conductivity by the effect of Brillouin zone folding or the scattering of phonons at the interlayer boundaries [17,21–23].

Recently, we reported the cross-plane thermal conductivity and boundary thermal resistance of thin-film superlattices in which a pure metal layer and a Fe_2VAl-based material layer were alternatively and periodically stacked [9]. All of the superlattices, except for that having the shortest period, had the same degree of dislocations near the interlayer boundaries, to realize similar interlayer heat resistance. In the sample of the small periods less than 20 nm, the thermal resistance at the interlayer boundaries decreased with decreasing periodic length because of the reduction in the number of dislocations with decreasing thickness of Fe_2VAl-based materials [9]. Besides, by making full use of the intensified interlayer boundary scattering, we succeeded to effectively reduce the thermal conductivity to as low as $3.4 \, W \, m^{-1} \, K^{-1}$ [9].

In this work, we tried to further reduce the lattice thermal conductivity of Fe_2VAl-based materials by simultaneously using the $5d$ heavy element partial substitution and the superlattice structure. The cross-plane thermal conductivities of superlattices containing a $5d$ element, W or Mo, were experimentally investigated, and the observed behavior was analyzed in terms of cumulative lattice thermal conductivity obtained from theoretical calculations. This work demonstrates that the $5d$ element substitution significantly contributes to reduce lattice thermal conductivity by modulating phonon dispersion and altering the interlayer boundary scatterings. We also reported a surprising fact that the $5d$ element substitution can be less effective for the reduction of lattice thermal conductivity in the superlattices with nanoscale periodic length less than 20 nm.

II. METHODS

In this work, we used four kinds of superlattice thin films consisting of four different materials, Fe_2VAl [9], $Fe_2(V, Ta)Al$, Mo, and W. $Fe_2(V, Ta)Al/M$ ($M =$ Mo, W) superlattices were grown as thin-film superlattices on the [100] MgO single-crystal substrates by means of a radio-frequency magnetron sputtering system (VTR-150F/SRF, Ulvac Kiko, Japan). A Mo layer of approximately 100 nm in thickness was deposited on the top and bottom sides of the superlattices to get the thermal diffusivity α by means of a time-domain thermoreflectance (TDTR) technique with a rear-heating front-detection (RF) configuration. A schematic drawing of the Fe_2VAl/metal superlattice is presented in Fig. 1. The total thicknesses L, the volume ratios of $Fe_2(V, Ta)Al$ to Mo or W, and the length of periodic unit P of the prepared samples are summarized in Table I.

The sputtering chamber was evacuated to below 2.0×10^{-4} Pa before starting the argon gas flow. During the deposition, the temperature of the substrate was kept at 873 K, the argon gas pressure at 2.0 Pa, and the RF power at 80 W. The growth rate of samples was estimated to be approximately 19 ($\pm$3) nm/min for the $Fe_2(V, Ta)Al$ and Mo layers, and
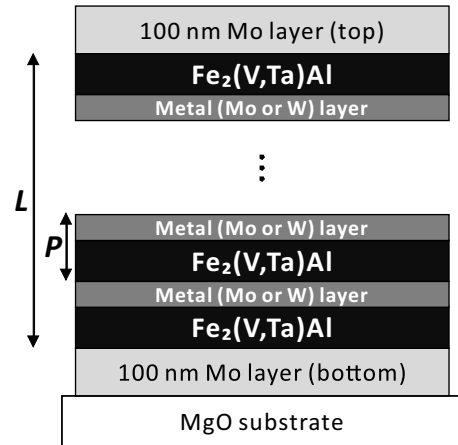

FIG. 1. Schematic drawings of the superlattice structure.

16 ($\pm$3) nm/min for the W layer. These numbers were estimated from the x-ray reflectometry analyses [24]. The solubility of Ta in the $Fe_2(V, Ta)Al$ layer was confirmed over 20 different locations of $Fe_2(V, Ta)Al$ single-layer thin film with thickness of more than 600 nm deposited on MgO at 873 K by means of the electron probe microanalysis (EPMA, JXA-8230, JEOL, Japan) at an accelerating voltage 15 kV and, thus, Ta content was 6.7 ± 0.4 at. % [25].

Out-of-plane x-ray diffraction (XRD) measurements in the range $20° – 80°$ using the Cu $K\alpha$ line (D8 Advance, Bruker, Germany). We also performed phi scan measurements for the MgO 202 and $Fe_2(V, Ta)Al$ 404 reflections.

The thermal transport properties along the cross-plane direction of superlattices were evaluated with a nanosecond pulsed-light heating time-domain thermoreflectance (TDTR) technique with the rf configuration (Nano-TR, PicoTherm, Japan). We deduced the cross-plane thermal conductivity $\kappa = dC\alpha$ for the superlattices using the thermal diffusivity α from the TDTR technique. Here d and C represent the averaged density and averaged specific heat of the whole $Fe_2(V, Ta)Al/M$ ($M =$ Mo, W) superlattices, respectively.

The calculations for both second- and third-order force constants were performed using $2 \times 2 \times 2$ supercells (64 atoms) comprising $1 \times 1 \times 2$ primitive cells and using 9760 supercells for $Fe_4V_2Al_2$ and 1800 supercells for Fe_4VTaAl_2 [25]. Real-space force constants of the supercell were calculated in the density functional perturbation theory (DFPT) implemented in the VASP code [26–29]. The generalized gradient approximation (GGA) of Perdew, Burke, and Ernzerhof (PBE) was used for the exchange correlation potential. A plane-wave energy cutoff of 500 eV was

TABLE I. Total thicknesses L, volume fractions V_{FVTA}/V_M of $Fe_2(V, Ta)Al$ and metal (Mo and W) layers, and periods P of the superlattice samples.

Superlattice	L (nm)	V_{FVTA}/V_M	P (nm)
$Fe_2(V, Ta)Al$/Mo	100	3/1	1.9, 2.5, 3.2, 6.3, 9.5, 19
	590	30/1	45, 59, 148, 295
$Fe_2(V, Ta)Al$/W	100	3/1	1.9, 3.2, 6.3, 9.5, 19
	590	30/1	45, 59, 148, 295
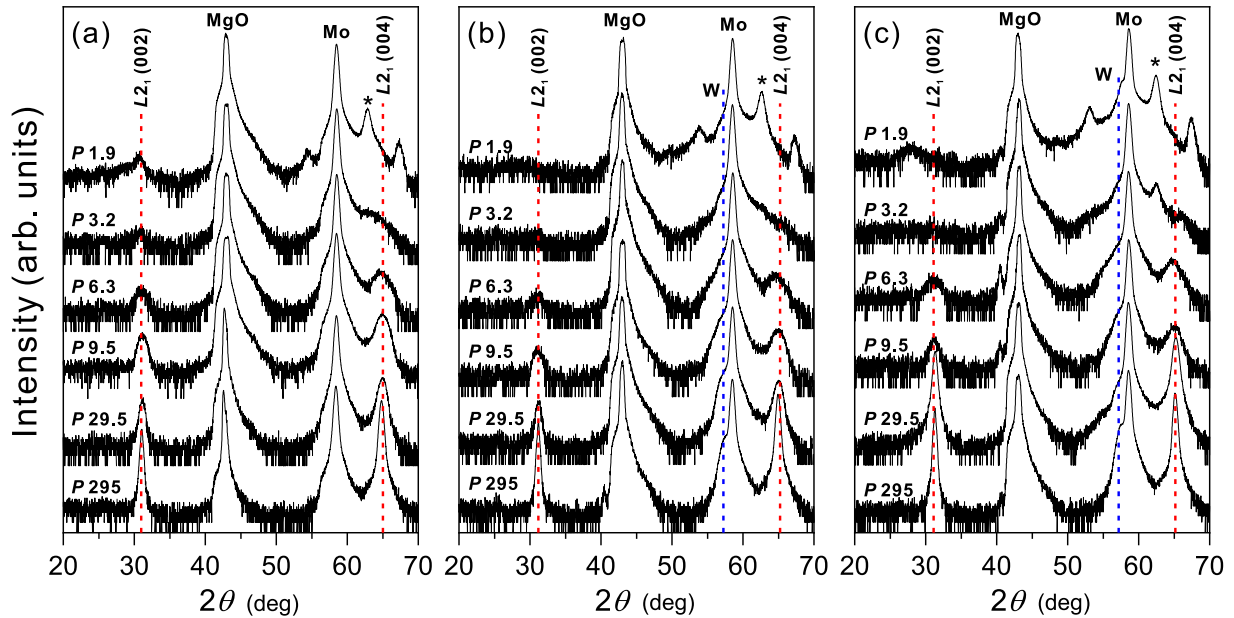
FIG. 2. Symmetric θ–2θ x-ray diffraction patterns of (a) $Fe_2(V, Ta)Al/Mo$ superlattices, (b) $Fe_2(V, Ta)Al/W$ superlattices, and (c) Fe_2VAl/W superlattices (reproduced from Ref. [9]) with varying period thickness at room temperature. Asterisk symbol is the zero-order satellite reflection. The unit of period number in each pattern is the nanometer.

employed throughout the calculations. The reciprocal space of the primitive cell of a $L2_1$-type structure was sampled using the $11 \times 11 \times 11$ mesh and the cumulative lattice thermal conductivities, $\kappa_{l,\mathrm{cum}}$, of $Fe_4V_2Al_2$ and Fe_4VTaAl_2 were calculated with the single-mode relaxation time approximation and linearized phonon Boltzmann equation using the PHONO3PY code [30–32].

III. RESULTS

Figures 2(a)–2(c) show the θ–2θ XRD patterns of $Fe_2(V, Ta)Al/Mo$ superlattices, $Fe_2(V, Ta)Al/W$ superlattices, and Fe_2VAl/W superlattices [9], respectively. The superlattices showed similar patterns for the same periodic length regardless of Ta substitutions or the inserted metal layer, Mo or W. This fact indicates a similar periodic length dependence in the quality of the crystal structure between the samples containing Mo and W layers. The relaxed $00l$ peaks in the superlattices with a period of $P > 19$ nm were slightly shifted to a low angle by Ta substitution from those of the Ta-free Fe_2VAl-based thin films [9,24]. The shift of the 004 peak corresponded to the lattice expansion of 0.0015 nm. This lattice expansion must have been brought about by the lattice parameter difference between 0.5777 nm of the sample containing 8 at. % of Ta and 0.5761 nm of nondoped Fe_2VAl bulk samples [6].

In the superlattices possessing a long period of $P > 6.3$ nm, the $00l$ peaks of the $L2_1$ phase were clearly observed in the XRD patterns regardless of Ta substitution. Notably, the full width at half maximum (FWHM) of those peaks decreased with increasing periodic length. This fact means that, even though the ordered $L2_1$ structure is constructed, the local atomic structure in the vicinity of interlayer boundaries is rather distorted. Besides, the volume fraction of portions

containing the heavy disordering was decreased with increasing thickness of the $L2_1$ structure.

In the superlattices with a short period of $P < 3.2$ nm, the $00l$ peaks disappeared presumably because the relaxed portions free from the heavy disordering were completely eliminated from the $L2_1$ layers. Surprisingly, the superlattices with the shortest period of 1.9 nm clearly possessed again the well-ordered $L2_1$ structure with 002 in the same manner as those in the samples of thicker periodic length of $P \geqslant 6.3$ nm, despite the 004 peak not being clearly observed in the samples of $P = 1.9$ nm, presumably because it was hidden in the background of the superlattice reflection peaks. Additionally considering the 004 peak was located at lower angles with satellite peaks, it is safely argued that the homogeneously strained but well-ordered $L2_1$ lattice would be formed in the limited regions being very close to the interlayer boundaries.

Note the large lattice mismatches between $Fe_2(V, Ta)Al$ and metal (Mo or W) layers, where the lattice mismatches, $\Delta a/a_M$, of $Fe_2(V, Ta)Al/Mo$ and $Fe_2(V, Ta)Al/W$ are approximately 7.9% and 9.2%, respectively. The observed diffraction angles of the satellite peak of $Fe_2(V, Ta)Al/Mo$ and $Fe_2(V, Ta)Al/W$ superlattices were $2\theta = 62.9°$ and $62.6°$, respectively. These diffraction angles corresponded to the lattice parameters of 0.5914 and 0.5934 nm, and smaller than 0.5953 nm ($2\theta = 62.4°$) in Fe_2VAl/W with lattice mismatch of $\sim 9.8\%$, which indicates that the large lattice mismatch led to a large peak shift [9].

Figures 3(a) and 3(b) show an in-plane azimuthal scan around the 202 peak of $Fe_2(V, Ta)Al$, indicating the epitaxial relation between the film and the substrate. Those peaks appear the fourfold symmetry and are located at 45° apart from the 202 peaks of the MgO substrate. The superlattices with a period of 1.9 nm show obviously sharp fourfold peaks, which are regarded as another evidence for the homogeneously strained but highly ordered $L2_1$ structure that has already
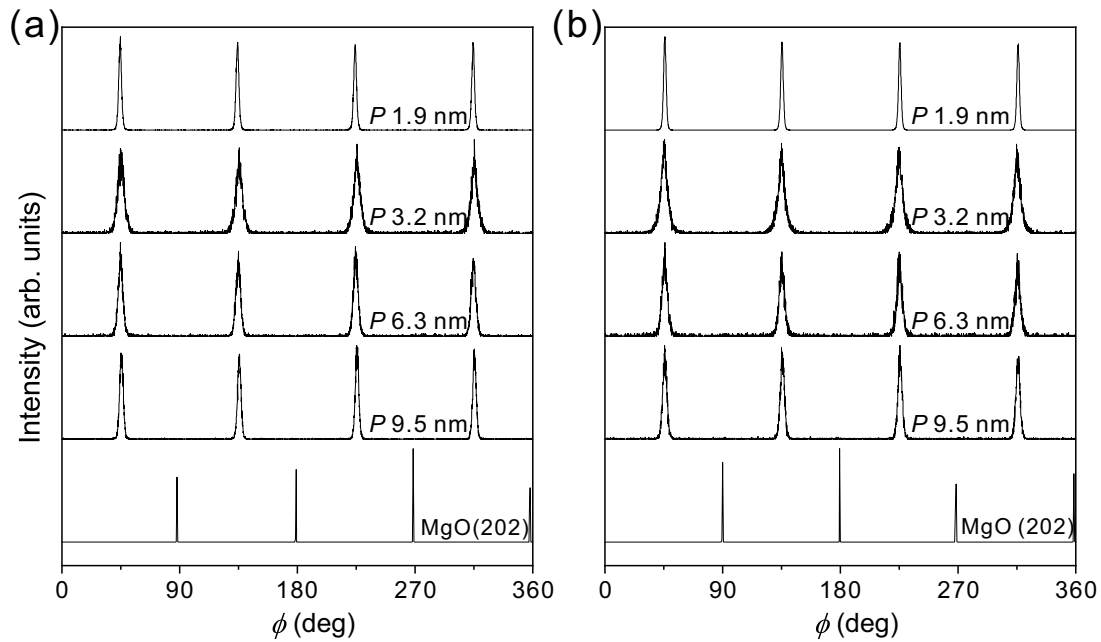
FIG. 3. Azimuthal scans around $Fe_2(V, Ta)Al$ 202 peak, MgO 202 peak, and zero-order satellite reflection near $Fe_2(V, Ta)Al$ 202 peak of (a) $Fe_2(V, Ta)Al$ /Mo superlattices and (b) $Fe_2(V, Ta)Al$/W superlattices at room temperature.

been confirmed from the sharp superlattice peaks shown in Figs. 2(a) and 2(b). The superlattices with a period of 3.2 nm have the broadest peak due to the intensified disordering mainly of dislocations that play a significant role in eliminating the strains. With further increasing periodic length, the FWHM of the peaks was getting narrowed most likely because the volume fraction of relaxed $L2_1$ structure increased.

To investigate the thermal transport properties in superlattices, TDTR measurements with the rear-heating, front-detection (RF) configuration were performed, and thus the temperature transient curves of $Fe_2(V, Ta)Al$/Mo and $Fe_2(V, Ta)Al$/W superlattices were obtained as shown in

Figs. 4(a) and 4(b). The solid black curves represent the result of function fitting by the analytical solution for a single-layer thin film derived from the mirror image method and the response function method [9,24,33,34]. Baba found out that the contribution of thermal resistance in each layer can be separated by use of the areal heat diffusion time of the thin film [34]. The areal heat diffusion time A is obtained from the area schematically drawn with a shaded area in Fig. 4(c) in which the injected heat is assumed to be used solely for heating the thin film but not to be conducted into the substrate. The details on the data analysis are given in the recently published papers [9,24].
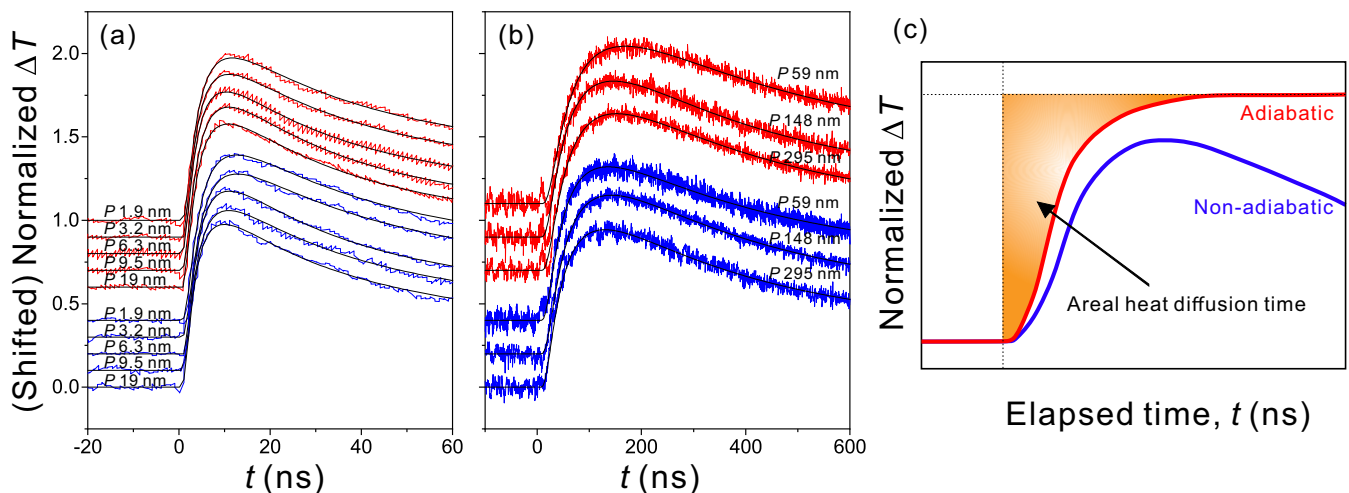

FIG. 4. Thermoreflectance signal curves with the results of black curves obtained by function fitting, of $Fe_2(V, Ta)Al$/Mo and $Fe_2(V, Ta)Al$/W superlattices with total thicknesses of (a) 100 nm and (b) 590 nm as a function of time at room temperature. (c) The definition of the areal heat diffusion time drawn as a shaded area.

TABLE II. A values of Mo/superlattice/Mo thin films obtained by function fitting for Figs. 4 (a) and 4(b).

P (nm)	Mo/[Fe$_2$(V, Ta)Al/Mo]$_n$/Mo (ns)	Mo/[Fe$_2$(V, Ta)Al/W]$_n$/Mo (ns)
1.9	4.38 ± 0.10	4.94 ± 0.15
2.5	4.19 ± 0.14	
3.2	4.28 ± 0.08	4.79 ± 0.15
6.3	4.04 ± 0.09	4.24 ± 0.09
9.5	3.87 ± 0.08	4.15 ± 0.12
19	4.05 ± 0.09	4.12 ± 0.10
45	48.65 ± 0.42	49.52 ± 0.60
59	48.45 ± 0.49	48.73 ± 0.71
148	48.07 ± 0.53	47.65 ± 0.53
295	46.73 ± 0.44	47.24 ± 0.32

We calculated the areal heat diffusion time A by assuming that the superlattice behaves as a single layer, and the results were summarized in Table II. For thin films having the same volume fraction and the same total thickness, the A value decreases slightly with increasing period, the likely signature of decreasing interface density. The A values became more than 10 times larger by simultaneously changing the volume fraction and total thickness, from 3/1 to 30/1 and from 100 to 590 nm, respectively.

The contributions of thermal resistance in the outer Mo and superlattice layers (SLs) were separated by the following equation [9].

$$A = \frac{\frac{(\frac{4}{3}+\Gamma)d_{Mo}^2}{\alpha_{Mo}} + \frac{(\frac{1}{\Gamma}+1+\Gamma/6)d_{SL}^2}{\alpha_{SL}}}{2+\Gamma}, \qquad (1)$$

where d and α are the thickness and the thermal diffusivity of each layer, respectively. Γ indicates the ratio of heat capacity

of the superlattice layer to that of the Mo layer, and is defined as $\Gamma = C_{SL}d_{SL}/C_{Mo}d_{Mo}$, where C represents the volumetric heat capacity estimated from both bulk density ρ and specific heat c_P of Mo [35], W [35], and Fe$_2$(V, Ta)Al. In the previous works, we have already confirmed that the boundary thermal resistance between the superlattice and the top or bottom Mo layer was nearly two orders smaller than the thermal resistance in superlattices. On that account, the contribution of boundary thermal resistance between the superlattice and the top or bottom Mo layer was ignored here [9,25]. From Eq. (1), we obtained the thermal diffusivity of superlattices α_{SL} which was used to estimate the thermal conductivity κ_{SL} of superlattices from $\kappa = \alpha\rho c_P$. The consequently obtained result was plotted in Fig. 5(a).

In Fig. 5(a), the measured thermal conductivity κ_{SL} of superlattices was plotted as a function of P. The average thermal conductivity of the Fe$_2$(V, Ta)Al-based superlattices with a period of $P \geqslant 19$ nm showed nearly constant values of $\sim 5.34(8)\,W\,m^{-1}\,K^{-1}$, which was comparable to the lattice thermal conductivities both of $\sim 5.70\,W\,m^{-1}\,K^{-1}$ for the Fe$_2$V$_{0.95}$Ta$_{0.05}$Al$_{0.95}$Si$_{0.05}$ bulk polycrystalline (PC) sample [3] and $\sim 5.20\,W\,m^{-1}\,K^{-1}$ for the Fe$_2$VAl$_{0.92}$Ta$_{0.08}$ bulk PC sample [6] at room temperature. This fact indicates that such a plateau region of the Fe$_2$(V, Ta)Al-based superlattices at $P \geqslant 19$ nm should be regarded as a bulk region. In the case of Ta-free Fe$_2$VAl-based superlattices, the bulk region is limited in the slightly longer P exceeding 200 nm. The thermal conductivity of such bulk regions should be dominated by the thermal conductivity of the relaxed $L2_1$ structure.

One can clearly observe in the plateau region of the highest lattice thermal conductivity that the Ta substitution led to a significant reduction in lattice thermal conductivity. The maximum reduction reached approximately 33%.

Surprisingly, the difference of the thermal conductivity between the Fe$_2$(V, Ta)Al-based samples and Fe$_2$VAl-based
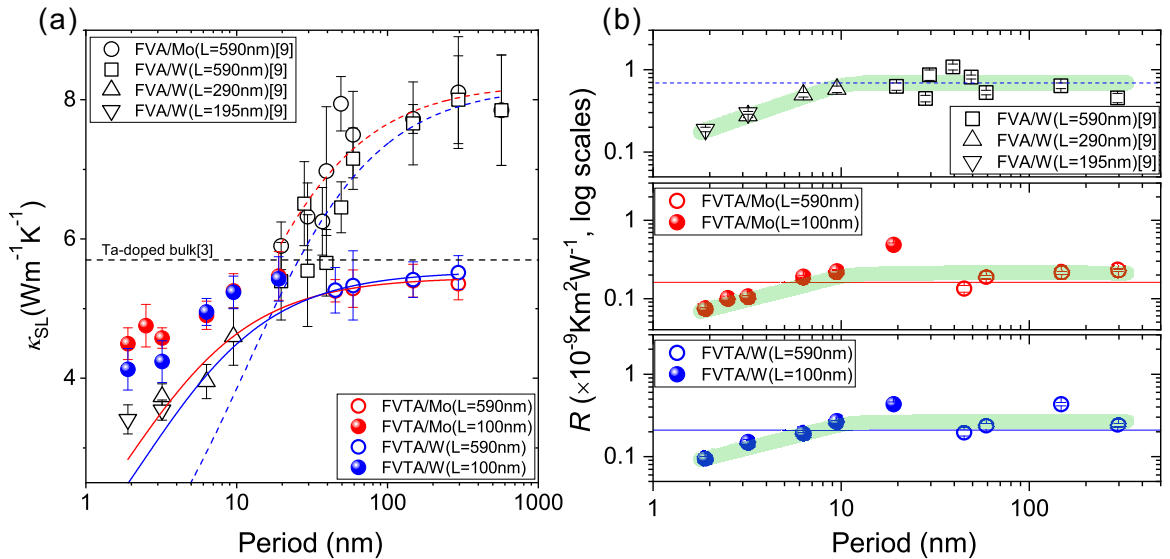

FIG. 5. (a) Cross-plane thermal conductivity and (b) boundary thermal resistance as a function of period or number of metal layers of Fe$_2$VAl [9] and Fe$_2$(V, Ta)Al-based superlattices as a function of period at room temperature. Dashed and solid curves of blue and red in (a) indicate the best fitting results calculated using Eq. (5) of superlattices with periods above 20 nm of Fe$_2$VAl and Fe$_2$(V, Ta)Al, respectively. Dashed and solid lines of blue and red in (b) indicate constant boundary thermal resistance of each series obtained from fitting (a). Thick solid curves of light green in (b) indicate the guideline.

samples became less obvious to be comparable with each other at the period of around $P = 20$ nm, and the Fe_2VAl-based samples turned out to possess smaller magnitude than the other at $P < 20$ nm. This fact was mainly caused by the rapid decrease of thermal conductivity with decreasing P in the Fe_2VAl-based superlattices. It is explained in other words that the phonons with a long mean free path in the Fe_2VAl-based superlattices are more effectively scattered by the introduced interlayer boundaries than those in the $Fe_2(V, Ta)Al$-based superlattices.

In the short period of $P < 20$ nm, the thermal conductivity of $Fe_2(V, Ta)Al$-based superlattices monotonically decreased with decreasing periodic length, but remained definitely larger than that of Fe_2VAl-based superlattices. According to the classic Klemens model on the low-frequency phonon scattering, the scattering probability τ^{-1} for phonons is inversely proportional to the scattering strength G [36]. Here τ and G are obtained as a function of the mass and concentration of impurity elements as follows.

$$\tau^{-1} = \frac{V\omega^4 G}{4\pi\upsilon^3}, \tag{2}$$

$$G = \sum_i c_i \left(\frac{M_i - M}{M}\right)^2, \tag{3}$$

where V, υ, and M represent the average atomic volume, mean phonon velocity, and average atomic mass, respectively. This relation means that the substitution by heavy impurity atoms would cause the variation in the thermal conductivity. These equations have been widely used to interpret the behavior of lattice thermal conductivity. Notably, however, the measured periodic length dependence of thermal conductivity, which is considered as mean free path dependence of lattice thermal conductivity, cannot be interpreted with these equations.

We initially expected that, even if the superlattice structure is constructed, a heavy element substituted compound would have lower lattice thermal conductivity than that of original nonsubstituted materials because of the strong scattering of phonons by the heavy element as explained in Eqs. (2) and (3). However, what we found in this study was that the lattice thermal conductivity was increased by the small amount of heavy element substitution in the Fe_2VAl-based superlattice at the short periodic length region $P > 20$ nm. Such a nontrivial behavior has rarely been reported. We speculated that this unique behavior would originate from the intrinsic phonon modes in $L2_1$ phases, and therefore performed phonon calculations and lattice thermal conductivity calculations. The calculation results are discussed in detail in Sec. IV (Discussion).

The thin region of $P < 20$ nm in all superlattice series has the abrupt variation in the quality of lattice as illustrated in Fig. 1(b) due to the large lattice mismatches between $Fe_2(V, Ta)Al$ and W (9.2%) and between $Fe_2(V, Ta)Al$ and Mo (7.9%). Thus, it is naturally considered that the larger lattice mismatch would cause stronger incoherency at the interlayer boundaries, and therefore additional misfit dislocations or other defects near interfaces are more significantly introduced in $Fe_2(V, Ta)Al$/W to reduce lattice thermal conductivity. If the mass difference between metal layers in superlattices was the dominant factor to determine the heat

transport, the difference between Mo and W in thermal conductivity should have appeared throughout the whole periodic length range, despite the tiny difference being found in the shortest range of periodic length [25]. Hence, we can safely argue that, in the thin region of $P < 3.5$ nm, the small difference of thermal conductivity between $Fe_2(V, Ta)Al$-based superlattices was caused by the difference in the degree of lattice mismatch between the $L2_1$ layers and the metal layers. In general, differences in the lattice mismatch, the bonding nature, and the atomic masses would lead to the finite variation in the acoustic phonon modes and scattering probability [25].

IV. DISCUSSION

To shed more light on the thermal transport in the superlattice samples, the thermal resistance of the superlattice is considered as the sum of inverse thermal conductivity in individual layers and that at the interlayer boundaries. The relation between the thermal conductivity κ_{SL} of the superlattice and the thermal resistance R at the interlayer boundaries is described in the following equation [13,22,25].

$$\kappa_{SL} = \frac{L}{n\left(\frac{d_{L2_1}}{\kappa_{L2_1}} + \frac{d_M}{\kappa_M} + 2R\right) + \frac{d_{L2_1}}{\kappa_{L2_1}}}, \tag{4}$$

where L is the total thickness of the superlattice, n is the number of metal layers in the superlattice, and d_{L2_1} and d_M are thicknesses of the $L2_1$ phase and metal layers in one unit layer, respectively.

Here, one can consider that the superlattices dominantly possessing the relaxed $L2_1$ structure may have mostly the same R values, because they have the same lattice structure near interfaces between $L2_1$ and metal layers as mentioned before. To verify the effect of this structural result for the thermal transport property, we assumed that, in superlattices with total thickness of 590 nm, the thermal conductivity of an individual $L2_1$ layer is equivalent to that of a $L2_1$ layer of 570 nm which is a sum for thicknesses of $L2_1$ layers in each superlattice. As shown in Fig. 5(a), the fitting parameters, $\kappa_{L2_1}^{fit}$ and R^{fit}, were obtained from the function fitting for κ_{SL} of superlattices with total thickness ~590 nm in each series using the following modified equation for Eq. (4) and listed in Table III.

$$\kappa_{SL} = \frac{590\ \text{nm}}{\frac{20\ \text{nm}}{\kappa_{L2_1}^{fit}} + \frac{570\ \text{nm}}{\kappa_M} + 2R^{fit}\frac{590\ \text{nm}}{P}}, \tag{5}$$

TABLE III. The thermal conductivity of $L2_1$ layer $\kappa_{L2_1}^{fit}$ and the constant boundary thermal resistance R^{fit} in superlattices obtained from fitting of Eq. (5) for each superlattice series in Fig. 5(a).

Superlattice	$\kappa_{L2_1}^{fit}$ (W m^{-1} K^{-1})	R^{fit} ($\times 10^{-10}$ K m^2 W^{-1})
Fe_2VAl/Mo [9]	7.98	4.70
Fe_2VAl/W [9]	7.94	6.90
$Fe_2(V, Ta)Al$/Mo	5.30 ± 0.01	1.61 ± 0.13
$Fe_2(V, Ta)Al$/W	5.38 ± 0.03	2.10 ± 0.35

where κ_{SL} is a dependent variable, period P is an independent variable, and κ_M is the bulk thermal conductivity for a metal layer in the superlattices [37].

The constant R^{fit} curves obtained from the function fitting show good consistency with the experimental data in the longer period of $P > 40$ nm. [See solid curves in Fig. 5(a).] The κ_{SL} of the superlattices in the period of $P < 20$ nm clearly showed larger values than the fitting curves for all series of samples, because the real value of boundary thermal resistance R was not kept constant but definitely varied due to the structure variation with thickness of layer. That was schematically drawn in Fig. 5(b). This result is very consistent with our recent work for the $L2_1$ thickness dependences of thermal transport in $L2_1$-based multilayer thin films [24,25].

From the fitting, we obtained the constant R^{fit} values of 1.61×10^{-10} m^2 K W^{-1} and 2.10×10^{-10} m^2 K W^{-1} for Fe$_2$(V, Ta)Al/Mo and Fe$_2$(V, Ta)Al/W superlattices, respectively, in the thicker range of $P > 40$ nm. We recently reported that the constant R^{fit} values of Fe$_2$VAl/Mo and Fe$_2$VAl/W superlattices were 4.70×10^{-10} m^2 K W^{-1} and 6.90×10^{-10} m^2 K W^{-1} for the range of $P > 20$ nm, respectively [9].

The ratio of R^{fit} in Fe$_2$VAl/Mo to that in Fe$_2$VAl/W was ~0.68, and that of Fe$_2$(V, Ta)Al/Mo to Fe$_2$(V, Ta)Al/W superlattices was ~0.77. Recently, we reported, by use of phonon calculation, that the phonon transmission probability ratios of Fe$_4$V$_2$Al$_2$/W to Fe$_4$V$_2$Al$_2$/Mo and that of Fe$_4$VTaAl$_2$/W to Fe$_4$VTaAl$_2$/Mo were ~0.58 and ~0.93, respectively [25]. Notably, those numbers were close to the obtained R^{fit} ratio. This indicates that such R^{fit} ratio closer to unity in Fe$_2$(V, Ta)Al-based superlattices might dominantly stem from the relaxation of phonon mismatching by a resonant mode caused from mass difference between Ta and V [25,38].

We obtained the R values of each data point by tentatively assuming that κ_{L2_1} in superlattices is equivalent to the $\kappa_{L2_1}^{fit}$ as aforementioned; these points were plotted as a function of periodic length in Fig. 5(b). In this result, all the superlattice series showed monotonically increasing R with increasing P and then stayed constant in the period of $P > 40$ nm. The constant tendency of R in the period of $P > 40$ nm would mainly be attributed to being of nearly uniform atomic structure including both strained and disordered $L2_1$ structures in the very thin portion near the interlayer boundaries.

In the period of $P < 20$ nm, the R values of Fe$_2$(V, Ta)Al-based superlattices were even lower than those of Fe$_2$VAl-based superlattices. As mentioned before, the lattice mismatch in Fe$_2$(V, Ta)Al/M ($M = $ Mo, W) was slightly lower than that in Fe$_2$VAl/W, which may contribute to a decrease of strain near interfaces resulting in a more ordered lattice structure. Simultaneously, the change of energy dependence of phonon modes induced by the Ta substitution changed the phonon mismatch between the $L2_1$ phase and the metal layer, which would also have contributed to the reduction of R values. The further reduction of R values in Fe$_2$(V, Ta)Al/Mo would mainly be due to the reduction of strain field in association with the lowest lattice mismatch. Thus, such a magnitude difference in boundary thermal resistance would be due to not only the difference of lattice mismatch between $L2_1$ and metal layers in superlattices but also the substitution of V by Ta site in the $L2_1$ layer.

In order to further discuss the experimental results, the lattice thermal conductivity was calculated using Boltzmann transport theory with the single-mode relaxation time approximation and is expressed as follows [32].

$$\kappa_l = \frac{1}{NV_0} \sum_\lambda C_\lambda v_\lambda \otimes v_\lambda \tau_\lambda, \tag{6}$$

where N is the number of unit cells in the system, V_0 is the volume of a unit cell, C_λ is the mode-dependent heat capacity, v_λ is the mode group velocity, and τ_λ is the mode relaxation time. The suffix λ represents the phonon mode as the pair of phonon wave vector $\mathbf{q}$ and branch j, $\lambda \equiv (\mathbf{q}, j)$. C_λ is expressed as follows.

$$C_\lambda = k_B \left(\frac{\hbar\omega_\lambda}{k_B T}\right)^2 \frac{\exp(\hbar\omega_\lambda/k_B T)}{[\exp(\hbar\omega_\lambda/k_B T) - 1]^2}, \tag{7}$$

where $\omega_\lambda = \omega(\mathbf{q}, j)$ is the frequency of the phonon mode λ, T is the temperature, $\hbar$ is the reduced Planck constant, and k_B is the Boltzmann constant. v_λ is defined as follows.

$$v_\lambda = \nabla_\mathbf{q}\omega(\mathbf{q}, j), \tag{8}$$

Here, it is assumed that the single-mode relaxation time τ_λ is used as the phonon lifetime which is computed from the imaginary part of phonon self-energy $\Gamma_\lambda(\omega_\lambda)$ and is defined as follows.

$$\tau_\lambda = \frac{1}{2\Gamma_\lambda(\omega)}, \tag{9}$$

$$\Gamma_\lambda(\omega) = \frac{18\pi}{\hbar^2} \sum_{\lambda'\lambda''} |\Phi_{-\lambda\lambda'\lambda''}|^2 \{(n_{\lambda'} + n_{\lambda''} + 1)\delta(\omega - \omega_{\lambda'} - \omega_{\lambda''})$$
$$+ (n_{\lambda'} - n_{\lambda''})[\delta(\omega + \omega_{\lambda'} - \omega_{\lambda''}) - \delta(\omega - \omega_{\lambda'} + \omega_{\lambda''})]\}, \tag{10}$$

where the strength of interaction between three phonon modes, $\Phi_{-\lambda\lambda'\lambda''}$, is obtained from the third-order interatomic force constant matrix and n_λ is the Bose-Einstein distribution, $n_\lambda = 1/[\exp(\hbar\omega_\lambda/k_B T) - 1]$.

The cumulative lattice thermal conductivity was obtained from the first-principles calculations with three phonon processes and can be simply described as a function of phonon mean free path as follows.

$$\kappa_{l,cum}(\lambda_0) = \int_0^{\lambda_0} \frac{d\kappa}{d\lambda} d\lambda, \tag{11}$$

where λ_0 is the threshold phonon mean free path corresponding to the onset length scale of phonon scattering and $\Delta\kappa_\lambda$ is the distribution function for the lattice thermal conductivity per unit mean free path.

Figure 6(a) shows cumulative lattice thermal conductivity $\kappa_{l,cum}(\lambda_0)$ calculated for Fe$_4$V$_2$Al$_2$ and Fe$_4$VTaAl$_2$. The most of conducting heat is carried by phonon modes with the mean free path both of less than 100 nm in Fe$_4$V$_2$Al$_2$ and those less than 20 nm for Fe$_4$VTaAl$_2$. Notably, although the calculation condition did not include scattering effects by imperfections such as misfit dislocation and other disorderings, the obtained data plotted in Fig. 6(a) showed fairly good consistency in the bulk thermal conductivity limit and the length where a magnitude crossover takes place between Fe$_2$VAl and
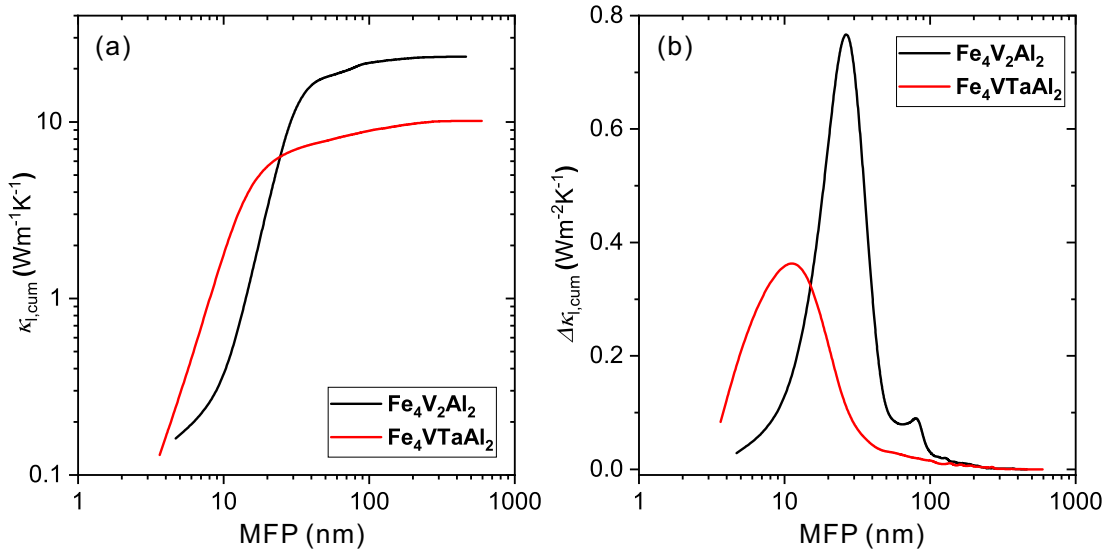
FIG. 6. (a) Cumulative lattice thermal conductivity $\kappa_{l,\mathrm{cum}}$ and (b) the derivatives $\Delta\kappa_{l,\mathrm{cum}}$ of (a) of $Fe_4V_2Al_2$ and Fe_4VTaAl_2 as a function of mean free path at 300 K.

$Fe_2(V, Ta)Al$. We confirmed that the shortest limit of bulk thermal conductivity in Fe_2VAl and $Fe_2(V, Ta)Al$ is 100 and 20 nm, respectively, both in calculations and experiments. Besides, the calculated cumulative lattice thermal conductivity $\kappa_{l,\mathrm{cum}}(\lambda_0)$ for Fe_2VAl and $Fe_2(V, Ta)Al$ plotted as a function of mean free path showed a magnitude crossover at around 20 nm in the same manner with the periodic length dependence of the measured thermal conductivity of the superlattice showing the magnitude crossover between sample with or without Ta in the $L2_1$ phase. Since the present calculation did not take the effect of impurity scatterings into account, our present result clearly indicated that the reduction of lattice thermal conductivity with a heavy element partial substitution is dominated by the variation of phonon dispersion and umklapp scattering rather than impurity scattering.

Using the vibrational density of states calculated $Fe_4V_2Al_2$ and Fe_4VTaAl_2, we argued in our previous paper that the significant reduction of thermal conductivity by heavy element substitution is attributed to the shift of optical phonon branches towards lower energy that leads to both the reduction of phonon group velocity and the enhanced umklapp processes [25]. To understand this effect more precisely, we calculated here the mean free path derivative of $\kappa_{l,\mathrm{cum}}(\lambda_0)$ because it should provide us with the mean free path dependence of thermal conductivity $\kappa(\lambda)$. The results are shown in Fig. 6(b).

The substitution of V by Ta leads to the remarkable change of dominant phonon modes of heat conduction such that the peak position in $\kappa(\lambda)$ is moved from 28 to 12 nm. Additionally the peak intensity of $\kappa(\lambda)$ is reduced by the Ta substitution for V. These facts mean that most of the phonons are more frequently scattered in the Fe_2VAl containing Ta and hence the mean free path is shortened to greatly reduce the heat conduction.

Once the condition mentioned above is realized by Ta substitution, one cannot further reduce the lattice thermal conductivity by using nanostructuring because of the absence of phonons having a long mean free path. This

fact definitely led to the observed crossover in the periodic dependence of thermal conductivity in the superlattice samples.

We should mention here the possible difference between the calculated cumulative lattice thermal conductivity $\kappa_{l,\mathrm{cum}}(\lambda_0)$ shown in Fig. 6(a) and the measured periodic dependence of thermal conductivity of superlattices $\kappa_{l\_SL}(P)$ shown in Fig. 5(a). The periodic length dependence of experimental lattice thermal conductivity $[\kappa_{l\_SL}(P)]$ should be described by the following formula.

$$\kappa_{l\_SL}(P) = \int_0^P \frac{d\kappa}{d\lambda}d\lambda + \alpha(P)\int_P^\infty \frac{d\kappa}{d\lambda}d\lambda. \quad (12)$$

We added the second term in Eq. (12) to involve the finite contribution of "phonons having a long mean free path and being scattered at the interlayer boundary" to the thermal conductivity. It is naturally considered that the contribution of the scattered phonons would be proportional to the number of phonons initially having the mean free path longer than P. The cumulative lattice thermal conductivity, on the other hand, is explained solely by the first term of Eq. (12). Such a difference in definition leads to difference in $\kappa_{l\_SL}(P)$ and $\kappa_{l,\mathrm{cum}}(\lambda_0)$.

It would be worthwhile mentioning the possible performance of Fe_2VAl-based thermoelectric materials. We obtained the lowest values of thermal conductivity of $\kappa = \sim 3.4\,\mathrm{W\,m^{-1}\,K^{-1}}$ and $\kappa = \sim 4.1\,\mathrm{W\,m^{-1}\,K^{-1}}$ from Fe_2VAl/W and $Fe_2(V, Ta)Al/W$ superlattices with the period of 1.9 nm, respectively. By assuming the power factor of $6.7\,\mathrm{mW\,m^{-1}\,K^{-2}}$ obtained from the $Fe_2V_{1.05}Al_{0.95}$ bulk at 300 K by Renard *et al.* [6], we could obtain the dimensionless figure of merit of $zT = 0.59$ and 0.49 from Fe_2VAl/W and $Fe_2(V, Ta)Al/W$ superlattices, respectively, whose values are approximately 4–5 times larger than the reported one ($zT = 0.12$). Finally, by assuming the maximum power factor of $46.7\,\mathrm{mW\,m^{-1}\,K^{-2}}$ obtained from a $Fe_2V_{0.8}W_{0.2}Al$ single-layer thin film at 338 K by Hinterleitner *et al.* [10], we can expect $zT = 4.12$ and 3.42 from Fe_2VAl/W and

$Fe_2(V, Ta)Al/W$ superlattices, respectively, whose values are comparable to the reported $zT = 5.86$ at 338 K.

V. CONCLUSION

We investigated cross-plane thermal conductivity of $Fe_2(V, Ta)Al/M(M = Mo, W)$ superlattices to gain insight into the effect of $5d$ heavy element substitution on the thermal transport of Fe_2VAl-based superlattices. The origin of experimentally observed reduction of thermal conductivity by $5d$ heavy element substitution was also analyzed by the theoretical calculations. For the samples possessing a long periodic length more than 20 nm, the $5d$ element substitution was definitely effective to reduce thermal conductivity of superlattices due to the increase of probability of umklapp scattering and reduction in mean group velocity. At the shorter periodic length less than 20 nm, the thermal conductivity of a $5d$ element free superlattice turned out to possess smaller thermal conductivity than the superlattices containing $5d$ elements.

We revealed that this surprising fact was well accounted for with the phonon distribution as a function of mean free path; phonons dominantly possessing a shorter mean free path in the samples containing $5d$ element prevented us from reducing lattice thermal conductivity by the nanostructuring. We conclude that heavy element substitution is an effective method for reducing lattice thermal conductivity of coarse grain samples, but has no synergy effect in combinational use with nanostructuring on the further reduction of lattice thermal conductivity.

[1] H. Miyazaki, S. Tanaka, N. Ide, K. Soda, and Y. Nishino, Mater. Res. Express **1**, 015901 (2013).

[2] Y. Nishino and Y. Tamada, J. Appl. Phys. **115**, 123707 (2014).

[3] Y. Terazawa, M. Mikami, T. Itoh, and T. Takeuchi, J. Electron. Mater. **41**, 1348 (2012).

[4] T. Takeuchi, Y. Terazawa, Y. Furuta, A. Yamamoto, and M. Mikami, J. Electron. Mater. **42**, 2084 (2013).

[5] Y. Furuta, K. Kato, T. Miyawaki, H. Asano, and T. Takeuchi, J. Electron. Mater. **43**, 2157 (2014).

[6] K. Renard, A. Mori, Y. Yamada, S. Tanaka, H. Miyazaki, and Y. Nishino, J. Appl. Phys. **115**, 033707 (2014).

[7] N. Fukatani, Y. Kurosaki, S. Yabuuchi, A. Nishide, and J. Hayakawa, Appl. Phys. Lett. **112**, 033902 (2018).

[8] S. Masuda, K. Tsuchiya, J. Qiang, H. Miyazaki, and Y. Nishino, J. Appl. Phys. **124**, 035106 (2018).

[9] S. Hiroi, S. Nishino, S. Choi, O. Seo, J. Kim, Y. Chen, C. Song, A. Tayal, O. Sakata, and T. Takeuchi, J. Appl. Phys. **125**, 225101 (2019).

[10] B. Hinterleitner, I. Knapp, M. Poneder, Y. Shi, H. Müller, G. Eguchi, C. Eisenmenger-Sittner, M. Stöger-Pollach, Y. Kakefuda, N. Kawamoto, Q. Guo, T. Baba, T. Mori, S. Ullah, X. Q. Chen, and E. Bauer, Nature **576**, 85 (2019).

[11] S. Yamada, K. Kudo, R. Okuhata, J. Chikada, Y. Nakamura, and K. Hamaya, Appl. Phys. Express **10**, 115802 (2017).

[12] K. Kudo, S. Yamada, J. Chikada, Y. Shimanuki, Y. Nakamura, and K. Hamaya, Jpn. J. Appl. Phys. **57**, 040306 (2018).

[13] M. V. Simkin and G. D. Mahan, Phys. Rev. Lett. **84**, 927 (2000).

[14] B. C. Daly, H. J. Maris, K. Imamura, and S. Tamura, Phys. Rev. B **66**, 024301 (2002).

[15] A. Chernatynskiy, R. W. Grimes, M. A. Zurbuchen, D. R. Clarke, and S. R. Phillpot, Appl. Phys. Lett. **95**, 161906 (2009).

[16] T. Zhu and E. Ertekin, Phys. Rev. B **90**, 195209 (2014).

[17] J. Ravichandran, A. K. Yadav, R. Cheaito, P. B. Rossen, A. Soukiassian, S. J. Suresha, J. C. Duda, B. M. Foley, C. Lee, Y. Zhu, A. W. Lichtenberger, J. E. Moore, D. A. Muller, D. G. Schlom, P. E. Hopkins, A. Majumdar, R. Ramesh, and M. A. Zurbuchen, Nat. Mater. **13**, 168 (2014).

[18] Y. Wang, H. Huang, and X. Ruan, Phys. Rev. B **90**, 165406 (2014).

[19] Y. Chen, D. Li, J. R. Lukes, Z. Ni, and M. Chen, Phys. Rev. B **72**, 174302 (2005).

[20] P. Chakraborty, L. Cao, and Y. Wang, Sci. Rep. **7**, 8134 (2017).

[21] R. Venkatasubramanian, Phys. Rev. B **61**, 3091 (2000).

[22] B. Saha, Y. R. Koh, J. Comparan, S. Sadasivam, J. L. Schroeder, M. Garbrecht, A. Mohammed, J. Birch, T. Fisher, A. Shakouri, and T. D. Sands, Phys. Rev. B **93**, 045311 (2016).

[23] R. Cheaito, C. A. Polanco, S. Addamane, J. Zhang, A. W. Ghosh, G. Balakrishnan, and P. E. Hopkins, Phys. Rev. B **97**, 085306 (2018).

[24] S. Hiroi, S. Choi, S. Nishino, O. Seo, Y. Chen, O. Sakata, and T. Takeuchi, J. Electron. Mater. **47**, 3113 (2017).

[25] S. Choi, S. Hiroi, M. Inukai, S. Nishino, R. Sobota, D. Byeon, M. Mikami, M. Matsunami, and T. Takeuchi, Phys. Rev. B **101**, 104312 (2020).

[26] G. Kresse and J. Hafner, Phys. Rev. B **47**, 558 (1993).

[27] G. Kresse and J. Furthmüller, Phys. Rev. B **54**, 11169 (1996).

[28] G. Kresse and J. Furthmüller, Comput. Mater. Sci. **6**, 15 (1996).

[29] G. Kresse and D. Joubert, Phys. Rev. B **59**, 1758 (1999).

[30] K. Mizokami, A. Togo, and I. Tanaka, Phys. Rev. B **97**, 224306 (2018).

[31] A. Togo and I. Tanaka, Scr. Mater. **108**, 1 (2015).

[32] A. Togo, L. Chaput, and I. Tanaka, Phys. Rev. B **91**, 094306 (2015).

[33] N. Taketoshi, T. Baba, and A. Ono, Meas. Sci. Technol. **12**, 2064 (2001).

[34] T. Baba, Jpn. J. Appl. Phys. **48**, 05EB04 (2009).

[35] *Thermophysical Properties Handbook*, edited by Japan Society of Thermophysical Properties (Yokendo Ltd., Tokyo, 2008) (in Japanese).

[36] P. G. Klemens, Proc. Phys. Soc., London, Sect, A **68**, 1113 (1955).

[37] Thermophysical Properties Database System, http://tpds.db. aist.go.jp/tpds-web/index.aspx.

[38] K. Kimura, K. Yamamoto, K. Hayashi, S. Tsutsui, N. Happo, S. Yamazoe, H. Miyazaki, S. Nakagami, J. R. Stellhorn, S. Hosokawa, T. Matsushita, H. Tajiri, A. K. R. Ang, and Y. Nishino, Phys. Rev. B **101**, 024302 (2020).